Int. J. New. Chem., 2020, Vol. 7, Issue 4, pp. 318-335.

International Journal of New Chemistry

Published online January 2020 in http://www.ijnc.ir/.

Open Access

Print ISSN: 2645-7237

Online ISSN: 2383-188x

Original Research Article

Exploration of the microstructures of two series of chromium–rich Mn–based alloys elaborated by casting

Patrice Berthod[1]*, Jean-Paul Gomis[2] and Synthia Annick Ozouaki Wora[2]

[1]*Institut Jean Lamour, Université de Lorraine, P.O. Box 50840-54011 Nancy, France

[2]Faculté des Sciences et Technologies, Université de Lorraine, P.O. Box 70239-54506 Vandoeuvre-lès-Nancy, France

Received: 2020-04-24 *Accepted: 2020-08-10* *Published: 2020-09-29*

ABSTRACT

Manganese is a rather abundant element on earth and alloys based on it may be unexpensive. Alloyed with chromium for corrosion resistance and with carbon and a strong carbide-former element Mn can be the base of new metallic materials with interesting properties. In this work it is aimed to try elaborating Mn-based alloys by foundry and, in case of successful results, to explore the obtained microstructures. Two series were considered, a first one of the Mn – 25wt.%Cr basis with increasing amount in carbon, and a second one with addition of both carbon and tantalum addition. These seven alloys were synthesized by high frequency induction melting and their microstructures were examined using electron microscopy. Thermodynamic calculations were carried out to better understand the microstructure formation. Results show that a double-phased matrix composed of two intermetallic compounds was obtained for all alloys, as well as chromium or tantalum carbides as soon as the carbon content was high enough. Cutting was hard and led to microcracks revealing lacks in toughness. The hardness is very high. It is concluded that the elaboration of such alloys by foundry pose some problems which must be solved, but is possible. The high hardness can be interesting for some applications but the toughness is to be improved. Outlooks of this work are the characterization of the corrosion behavior of these alloys and of their mechanical properties.

Keywords: Manganese-based alloys; carbon; chromium; tantalum; foundry; microstructures; hardness

Introduction

In the Mendeleiev's Periodic Table of the elements, Manganese is in the same line of transition metals as chromium on the left and iron, cobalt, nickel on the right. Manganese is often met in small quantities associated to iron (few weight percent) in many steels, but also in some creep-resistant steels, with higher contents [1,2]. In alloys other than steels, manganese can be associated to other elements than iron, such aluminum [3,4], copper [5] and even precious metals [6], for instance. In association with these elements Mn is present in particular alloys such as alloys with soft magnetic properties [7], shape memory alloys [8,9], dental alloys [10], alloys with low thermal expansion [11], quasicrystals [12], amorphous alloys [7] and even composites [13]. In contrast, it is difficult to find manganese alloyed with chromium. Very old alloys involved Mn with Cr and Fe [14,15] and much recently NiCrMn alloys [16] were under consideration [16], but they are seemingly almost the alone ones.

There are four crystalline networks for pure manganese and they are all cubic. One of them is body centered cubic (BCC) as chromium, from 1160°C to the melting point. It is possible to think that adding Cr to Mn may promote the later crystalline structure and give cubic solid solutions. Consequently one can expect, in this hypothesis, that high ductility can be achieved by the existence of 12 sliding system homogeneously scattered directions for dislocation movement under stress, even for temperatures not too low. Such a BCC network is not as compact as Face Centered Cubic (FCC) structures, and thus not so mechanically resistant, but strength may be improved by hardening. The presence or addition of carbide-forming elements may lead to carbides if carbon is also added.

The purpose of this work is, first to discover the theoretical structure of binary Mn–Cr alloys, and second to concretely explore the microstructures of binary alloys made of manganese (base element) and chromium (as alloying element), of ternary alloys with addition of carbon in various contents, and to finish quaternary alloys with the addition of a strong carbide-forming element, tantalum. The choice of this later element takes its origin in its efficiency to form script-like eutectic carbides in various bases involving also chromium: cobalt–base superalloys [17], nickel–base superalloys [18], ferritic [19] or austenitic [20] steels.

Experimental

Thermodynamic calculations prior to elaboration

Preliminarily thermodynamic calculations were carried out to explore the theoretic constitutions of alloys based on manganese and containing significant quantities of chromium. This was done using the Thermo–Calc software (N version). Unfortunately thermodata were lacking for calculations in the Mn–Cr–C–Ta system and even in the Mn–Cr–C ternary one. Calculations were thus performed only on the binary Mn–Cr system, the description of which was available in the KP database. This allowed obtaining the high temperature part of the Mn–rich side of the Mn–Cr diagram. The evolution of the different phases from single liquid down to rather low temperatures were successfully obtained.

Elaboration of the two series of alloys

The chemical compositions were chosen: 25wt.%Cr for all alloys, 0, 0.25, 0.5 and 1 wt.%C for the binary and the three ternary alloys, 0.25C–3Ta, 0.5C–3Ta and 0.5C–6Ta (all contents in wt.%) for the three quaternary alloys. These contents are typical of the corresponding ones in superalloys, corrosion – resistant at ambient temperature and high temperatures (up to 1000°C and even more) and efficiently strengthened by carbides at elevated temperatures (up to 1200°C).

Taking into account that the capacity of the furnace available for these syntheses was of 50 grams mavximum, it was chosen to limit the charges to 40 grams. They were prepared with pure elements (flakes of Mn, small blocky parts of Cr and of Ta, graphite for C) with purities higher than 99.9% (supplier: Alfa Aesar). The masses in the different elements were carefully weighed using a precision balance (accuracy: ±0.1mg). Each charge was thus placed in the metallic segmented crucible of the furnace (made of copper, internally cooled by a continuous flow of water at ambient temperature). A transparent tube made of silica was placed around the crucible containing the charge, and the fusion chamber was closed and vacuumed down to less than 5×10^{-2} millibars. Pure argon was then introduced until reaching an internal pressure lower than but close to one atmosphere. Vacuuming and pure Ar introduction were repeated two times more, and the internal pressure was fixed at about 500 millibars of Ar.

Melting was achieved by progressively increasing up to 4 kV the voltage of the 110kHz alternative current. Melting occurred simultaneously with the intensive formation of dark vapors inside. A three minutes stage at the maximum voltage was done to chemically homogenize the liquid sphere levitating over the crucible (liquid maintained with this shape and without direct contact with copper by the electromagnetic forces). AT the end of these three minutes the applied voltage was progressively decreased, allowing the liquid alloy cooling and solidification. Solidification finished in contact with the copper crucible.

Metallographic examination of the obtained alloys

Each obtained egg-shaped ingot was cut in four sectors using a rotating abrasive wheel and samples for the metallographic examination were machined using a metallographic saw. The sections were examined a first time with the naked eye. The samples were embedded in a cold mixture made by the mix of 82% of liquid resin and of 18% of liquid hardener (ESCIL, France). After total stiffening the embedded samples were extracted from the plastic molds and ground with SiC papers under water (grades from 240# to 1200#). After ultrasonic cleaning and washing under water then alcohol (to remove eventual abrasive particles inherited from the SiC paers), final polishing was performed with textile disks enriched with 1µm alumina particles.

The mirror-like surfaces were examined again with the naked eye, then placed in a Scanning Electron Microscope (SEM), a JEOL JSM-6010LA one (Japan). The samples were then observed at different high magnifications in the Secondary Electrons (SE) mode and in the Back Scattered Electrons (BSE) mode. Control of the global chemical composition was achieved by full frame Energy Dispersive Analysis (EDS) on several areas with the ×250 magnification, and spot EDS analysis was carried out on the different phases or particles existing in the alloys.

Hardness measurements

Per sample up to 10 indentations were carried out under a 10kg – load and according to the Vickers procedures. The average value of hardness and the standard deviation one were then calculated.

Results and discussion

Thermodynamic calculations

A part of the Mn–richest half of the phase diagram of the binary Mn – Cr system, computed with Thermo–Calc, is presented in Figure 1. This phase diagram is rather complex since, over the 10–40% wt.%Cr and 800–1800K ranges, Thermo–Calc found three allotropic varieties of the Mn–based solid solution, two intermetallic compounds $Mn_{79}Cr_{21}$ and Mn_2Cr, two peritectic points and a peritectoïd point. The corresponding peritectic and peritectoïd reactions are the following ones:

- Liquid + $Mn_{79}Cr_{21}$ → Mn_{BCC}
- Liquid + Cr_{BCC} → $Mn_{79}Cr_{21}$
- Cr_{BCC} + $Mn_{79}Cr_{21}$ → Mn_2Cr

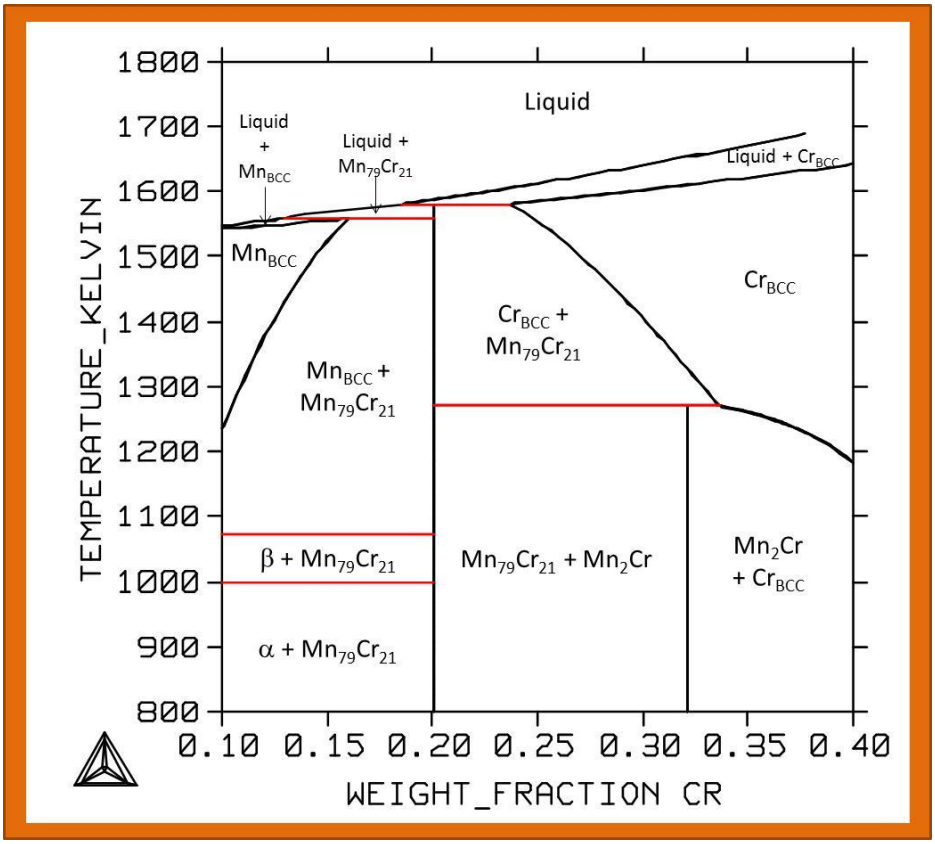

Figure 1. The binary Mn–Cr diagram (computed by Thermo-Calc N with the KP database)

In the same frame of the Mn – Cr diagram one can see that the Mn–rich solid solution may know two allotropic reactions during cooling: $Mn_{BCC} \rightarrow \beta \rightarrow \alpha$. Obviously there is no communications between the Cr–rich Mn–based BCC solid solution (named Mn_{BCC} here) and the Mn–rich Cr–based BCC solid solution (named Cr_{BCC} here), and the Mn–25wt.%Cr alloy should be formed of about 3/5 of $Mn_{79}Cr_{21}$ and 2/5 of Mn_2Cr. These phases being intermetallic one can threat that this alloy will be brittle at room temperature, and probably also many of the other alloys with C and/or Ta additions.

Microstructures of the alloys with 0.25wt.%C

The SEM/BSE images of the two alloys containing 0.25wt.%C without or with 3wt.%Ta (targeted contents), respectively named MCC1 and MCC1T, are presented together in Figure 2 (low magnification for general view) and in Figure 3 (high magnification for detailed view). The ternary MCC1 alloy obviously presents a double-phased matrix and small black precipitates. The microstructure of the quaternary MCC1T alloy does not really look like the MCC1 one but one find in its case too a double-phased matrix and small white particles. In both cases, considering the two gray levels seen in the matrix and remembering that these micrographs were taken in BSE mode, matrix seems to be composed of a dark phase with an average atomic number a little lower and of a brighter phase with an average atomic number a little greater. The black precipitates observed in the first alloy can be chromium carbides while the white precipitates dispersed in the second alloy can be tantalum carbides.

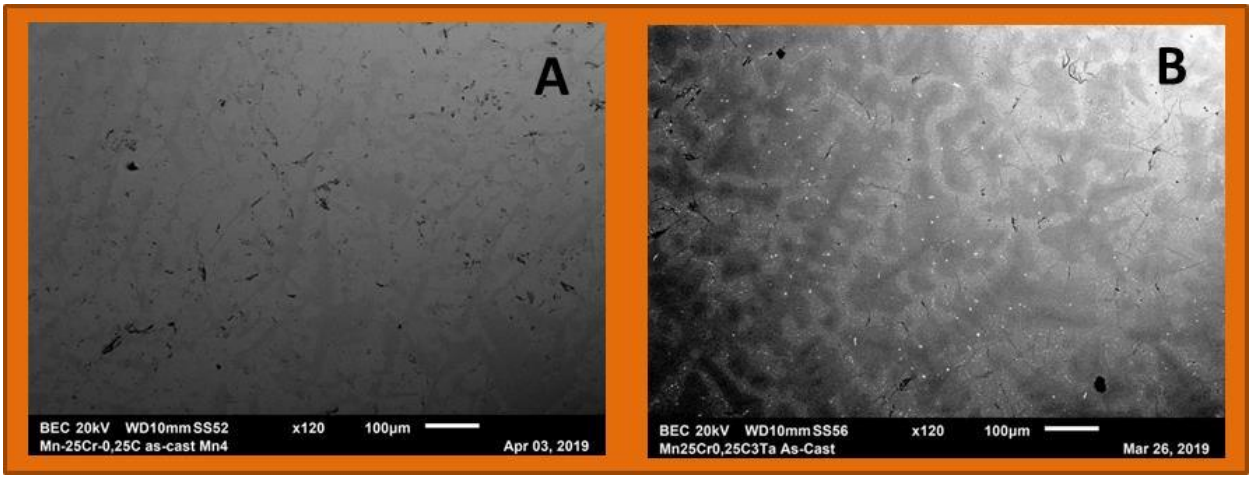

Figure 2. Microstructures of the MCC1 (A) and MCC1T (B) alloys (SEM/BSE mode, low magnification)

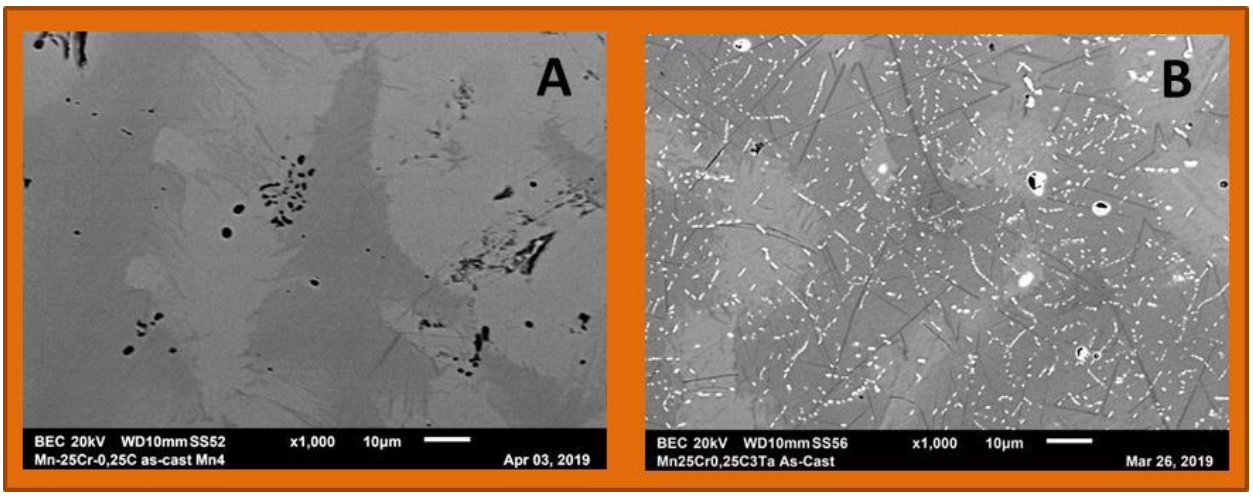

Figure 3. Microstructures of the MCC1 (A) and MCC1T (B) alloys (SEM/BSE mode, high magnification)

Microstructures of the alloys with 0.5wt.%C

A general view of the microstructures with 0.5wt.%C, without or with Ta is given in Figure 4.

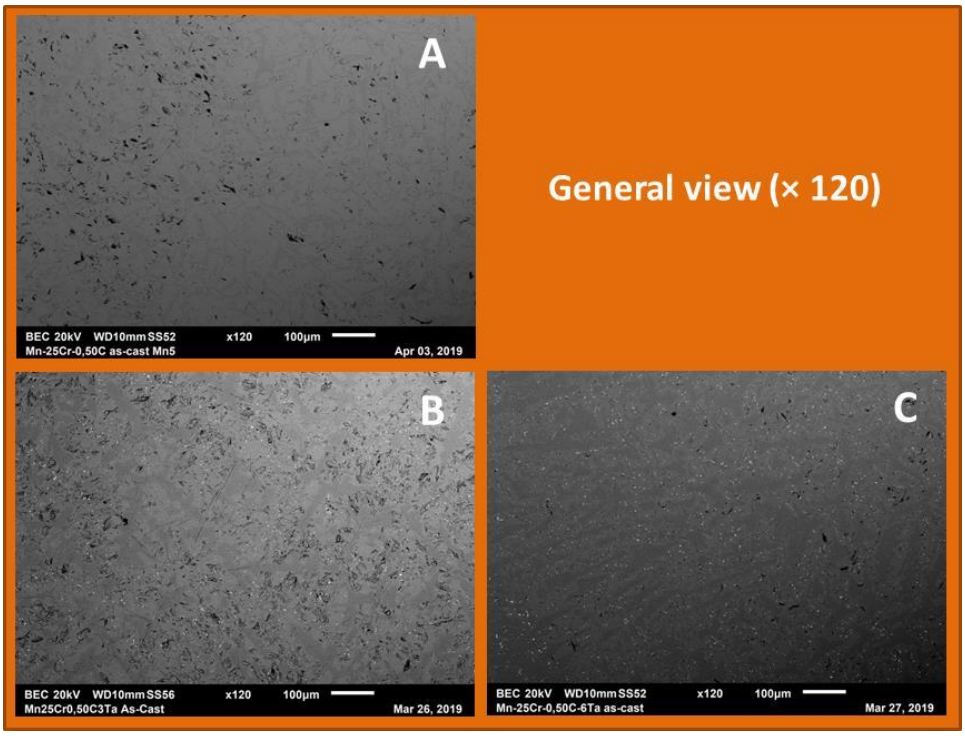

Figure 4. Microstructures of the MCC2 (A), MCC2T (B) and MCC2T' (C) alloys (SEM/BSE mode, low magnification)

These alloys, with as targeted compositions 0.5wt.%C (alloy named MCC2), 0.5wt.%C–3wt.%Ta (alloy named MCC2T) and 0.5wt.%C–6wt.%Ta (alloy named MCC2T'), are of the same type as the former ones but richer in black particles and/or white particles. Detailed views are provided in Figure 5. In all alloys one can again distinguishing two phases of matrix with two different average atomic numbers then two gray levels. In contrast with the 0.25wt.%C–containing alloys, the surface fraction of the dark particles are higher and their morphologies more complex. Concerning the white particles present in the MCC2T and MCC2T' alloys, they are only a little coarser than in the MCC1T alloy.

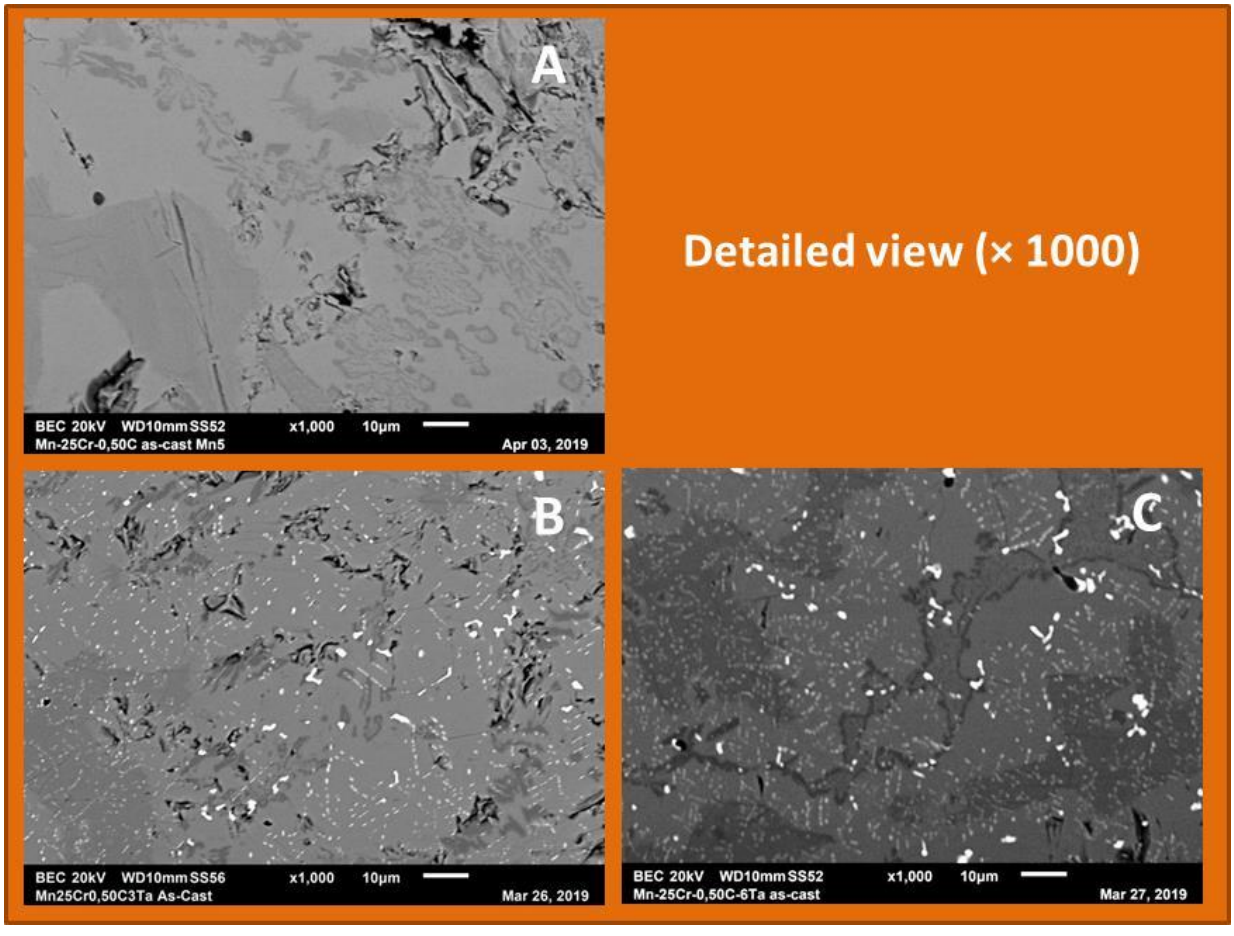

Figure 5. Microstructures of the MCC2 (A), MCC2T (B) and MCC2T' (C) alloys (SEM/BSE mode, high magnification)

Microstructures of the four Ta – free alloys

The detailed microstructures of the two other alloys, the binary one (named MC) and the carbon–richest one (named MCC3), are presented in Figure 6 in which their SEM/BSE micrographs taken with a medium magnification, are gathered with the micrographs of the 0.25wt.%C– or 0.5wt.%C–containing alloys already commented, to facilitate comparison and the analysis of the influence of the carbon content. Preliminarily one must remark that some of the alloys are affected by the presence of microcracks, which are here better seen than in micrographs with lower magnification. Second, other dark particles are present beside these microcracks, and they are more present when the carbon content increases. When the carbon content is the highest (1wt.%C) it is obvious that then this darkest phase is a chromium carbide which appeared at solidification by forming a eutectic compound with the matrix, morphologically very similar to Cr_7C_3 eutectic carbides encountered in some cobalt–based and nickel–based alloys.

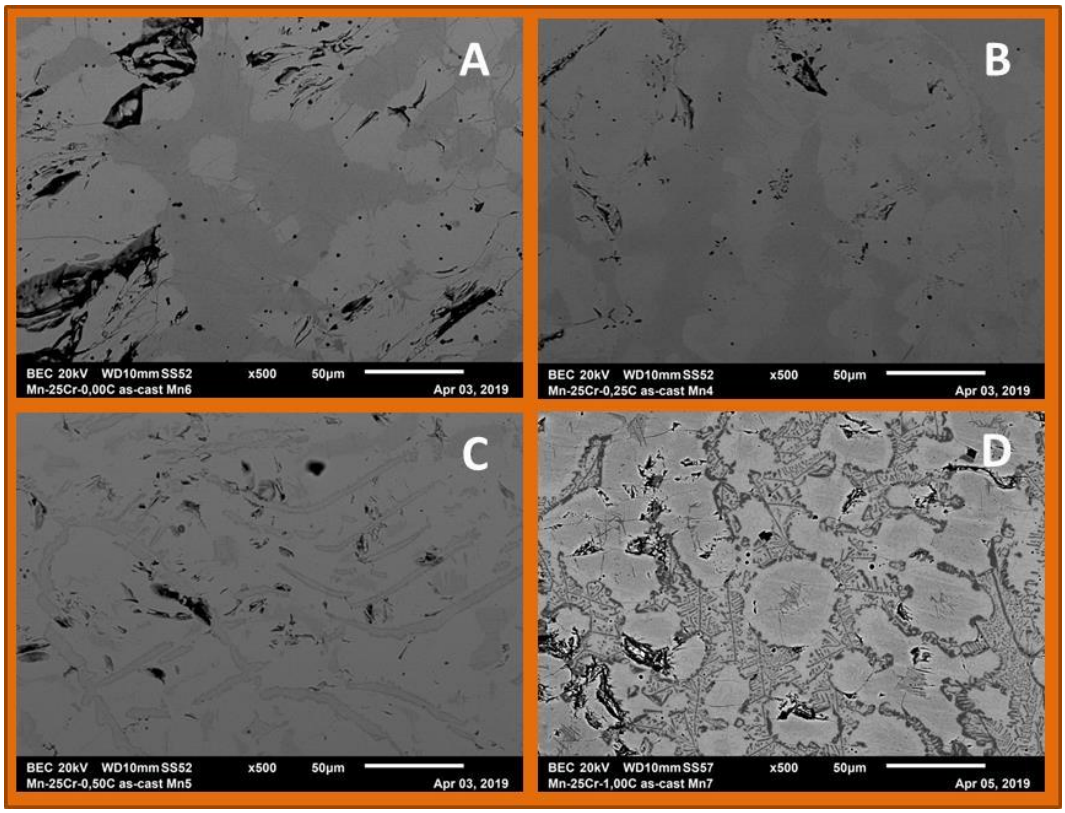

Figure 6. Microstructures of the MC (A), MCC1 (B), MCC2 (C) and MCC3 (D) alloys (SEM/BSE mode, medium magnification)

Chemical compositions of the obtained alloys

EDS full frame analysis, excluding carbon because its too low atomic mass and its too low contents in the alloys, was carried out on five areas randomly chosen in each sample. The results, present in Table 1, demonstrated that the wished chemical compositions were not really obtained. The most curious result concerns chromium. It is several points higher than expected. In fact this is due to the volatilization of manganese which happened during the melting. Indeed its evaporation point is much lower than the chromium and tantalum ones. The formation of Mn vapor due to the high level of temperature reached during melting (about 2000 K) led to the dense smoke continuously forming in the fusion chamber. Manganese was present in the powders deposited on the internal faces of the cold components inside the fusion chamber.

Table 1. Chemical compositions of the seven alloys (average and standard deviation values from five ×250 full frame EDS analysis); C supposed well respected (*: cannot be specified by full frame EDS); contents in wt.%

Alloy	Mn	C	Cr	Ta
MC	Bal.	0*	27.5 ± 0.8	/
MCC1	Bal.	0.25*	28.6 ± 0.4	/
MCC2	Bal.	0.50*	29.2 ± 0.5	/
MCC3	Bal.	1.00*	28.4 ± 0.6	/
MCC1T	Bal.	0.25*	29.5 ± 1.6	1.1 ± 0.4
MCC2T	Bal.	0.50*	28.1 ± 0.6	1.7 ± 0.3
MCC2T’	Bal.	0.50*	29.1 ± 0.4	2.3 ± 0.2

A second particular point to note in Table 1 is the low level of tantalum content in the alloys initially designed to contain either 3wt.%Ta (MCC1T and MCC2T alloys) or 6wt.%Ta (MCC2T' alloy). Due to its very high evaporation point tantalum it was not possible that a part of tantalum was lost by evaporation. On the contrary, due to significant manganese loss as vapor, the contents in Ta ought to higher than expected, as for chromium. These obtained Ta contents significantly lower than targeted were explained by looking to the remaining and not exploited cut parts of the MCC1T, MCC2T and MCC2T'alloys: presence of not melted parts of pure tantalum. Obviously, interdiffusion between the pure Ta parts and the formed Mn–Cr liquid did not progress enough or did to led to intermediate compounds with melting points low enough. Thus, only a part of tantalum really dissolved in the liquid and thus took part to the final Mn–Cr–C–Ta alloy. Concerning carbon, it was not possible to specify its content in the alloy, because of its low atomic mass but overall to its necessarily too low content in the whole alloys, even for the 1wt.%C–containing alloy (MCC3). In contrast, EDS spot analysis carried out on the coarsest dark particles or white particles found in the metallographic samples, by rating carefully the parameters of the electron beam, allowed rather accurate measurements of the C contents of these particles. This allowed identifying the darkest particles as being Cr_7C_3 carbides and the brightest ones as being TaC carbides. Due to their white tint, it was possible to measure their surface fraction using the image analysis tool of the Photoshop CS software of Adobe. The obtained results are located in the {1.5 – 4 surf.%} for the three alloys taken together.

Chemical compositions of the two phase of the matrixes

EDS spot analyses performed on the slightly brighter part of the matrix and on the slightly darker part of the matrix led to results which are summarized in Table 2 for the first matrix phase and in Table 3 for the second matrix part. The chromium content in the bright phase is globally lower than the one of the whole alloy while the chromium content in the dark phase is higher than the alloys' one. By reminding that the atomic mass of chromium is a little lower than the one of manganese one understands the order of gray levels between the two phases of the matrix. The bright matrix, with its between 24 and 28 wt.%Cr, do not correspond to one of the two intermetallic compounds expected by the results of Thermo-Calc calculations. This is different for the dark phase the Cr, content of which (from 32.5 to 36 wt.%) is rather close to the Mn_2Cr intermetallic. If one can admit that the dark phase is really Mn_2Cr, what is the bright phase?

Maybe another intermetallic compounds not predicted in the KP database? Or maybe there is a rather large Cr content solubility range for the $Mn_{79}Cr_{21}$ intermetallic?

Table 2. Chemical compositions of the bright part of the matrix in the seven alloys (average and standard deviation values from five spot EDS analysis); contents in wt.%

Alloy	Mn	C	Cr	Ta
MC	Bal.	0*	24.9 ± 2.3	/
MCC1	Bal.	0.25*	27.9 ± 1.0	/
MCC2	Bal.	0.50*	27.8 ± 1.1	/
MCC3	Bal.	1.00*	24.3 ± 3.8	/
MCC1T	Bal.	0.25*	25.9 ± 1.3	0.3 ± 0.2
MCC2T	Bal.	0.50*	25.8 ± 1.3	1.5 ± 1.7
MCC2T’	Bal.	0.50*	25.9 ± 1.3	0.3 ± 0.1

(*: cannot be specified by spot EDS on phase with low carbon contents)

Table 3. Chemical compositions of the dark part of the matrix in the seven alloys (average and standard deviation values from five spot EDS analysis); contents in wt.%

Alloy	Mn	C	Cr	Ta
MC	Bal.	0*	35.9 ± 2.3	/
MCC1	Bal.	0.25*	33.3 ± 1.5	/
MCC2	Bal.	0.50*	33.6 ± 2.0	/
MCC3	Bal.	1.00*	No dark phase	/
MCC1T	Bal.	0.25*	32.5 ± 1.5	0.1 ± 0.1
MCC2T	Bal.	0.50*	31.6 ± 2.0	0.3 ± 0.3
MCC2T’	Bal.	0.50*	31.9 ± 1.3	0.9 ± 0.9

(*: cannot be specified by spot EDS on phase with low carbon contents)

Hardness

The hardness values obtained for all alloys are graphically given in Figure 7, organized to facilitate the study of the dependence on the carbon content and on the tantalum one. As shown in Figure 7-A hardness increases with the carbon content while, according to Figure 7-B it seems also to be favored by tantalum. Since the hardness is seemingly the same for 0.25wt.%C without (MCC1 alloy) or with Ta (MCC1T), the nature of the carbides, chromium carbides or tantalum carbides, does not have any effect. The comparison between the MCC2T et MCC2T' alloys suggests that either there is no effect for such low variation in Ta contents, or the presence of more Ta (as carbides and/or in solid solution) tends slightly increasing hardness.

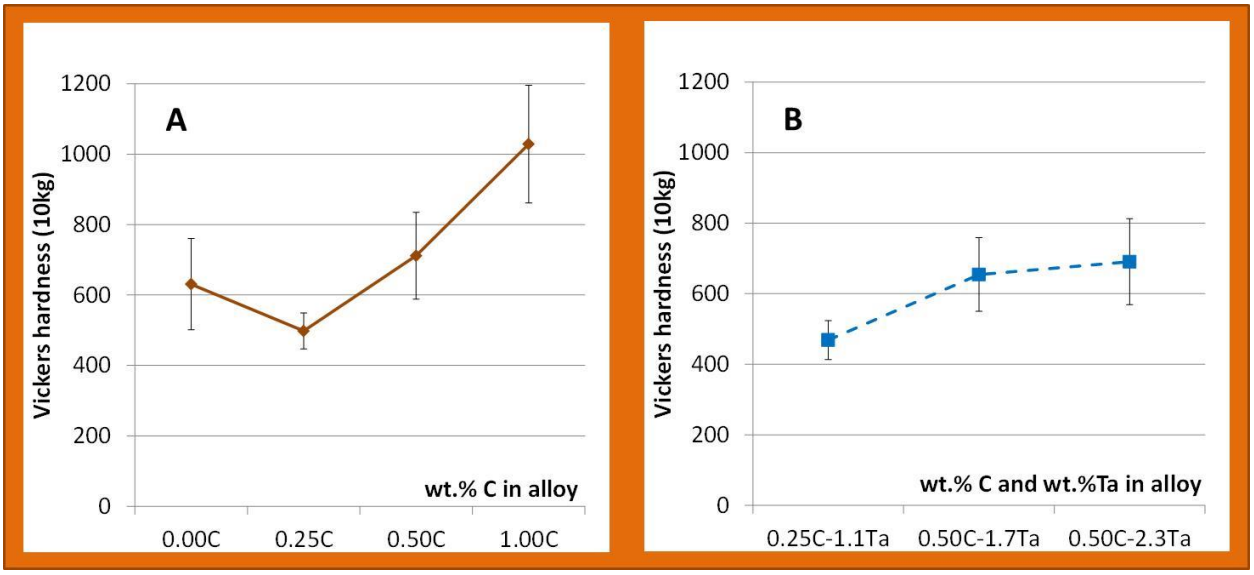

Figure 7. Hardness evolution versus the C content (A) and the C and Ta contents (B) (Vickers indentations under a 10 kg load)

Additional thermodynamic calculations

Knowing now, thanks to the global EDS results, the real chromium contents obtained in the alloys, on can attempt to have more quantitative data by the mean of Thermo–Calc. The real composition of the MC alloy (27.5wt.%Cr) was taken for calculating the mass fraction evolution for the different phases during

solidification and solid state cooling. The corresponding obtained results, graphically represented in Figure 8, show that solidification should start with the crystallization of the BCC Cr–based phase between 1340°C (liquidus temperature) and 1312°C (solidus temperature). The alloy remains single-phased between 1312°C and 1227°C, composed only of the BCC Cr–based phase. At 1227°C and below, the $Mn_{79}Cr_{21}$ intermetallic compound should nucleate and grow at the expense of the BCC Cr–based phase. When both phases arrive to be almost equivalent (55 mass.% of BCC Cr–based phase and 45 mass.% of $Mn_{79}Cr_{21}$ intermetallic), the peritectoïd reaction should proceed, isothermally (at 997°C). At the end of reaction the alloy is composed of 38 mass.% of $Mn_{79}Cr_{21}$ and 62 mass.% of Mn_2Cr, proportions which remain fixed down to 500°C and maybe below.

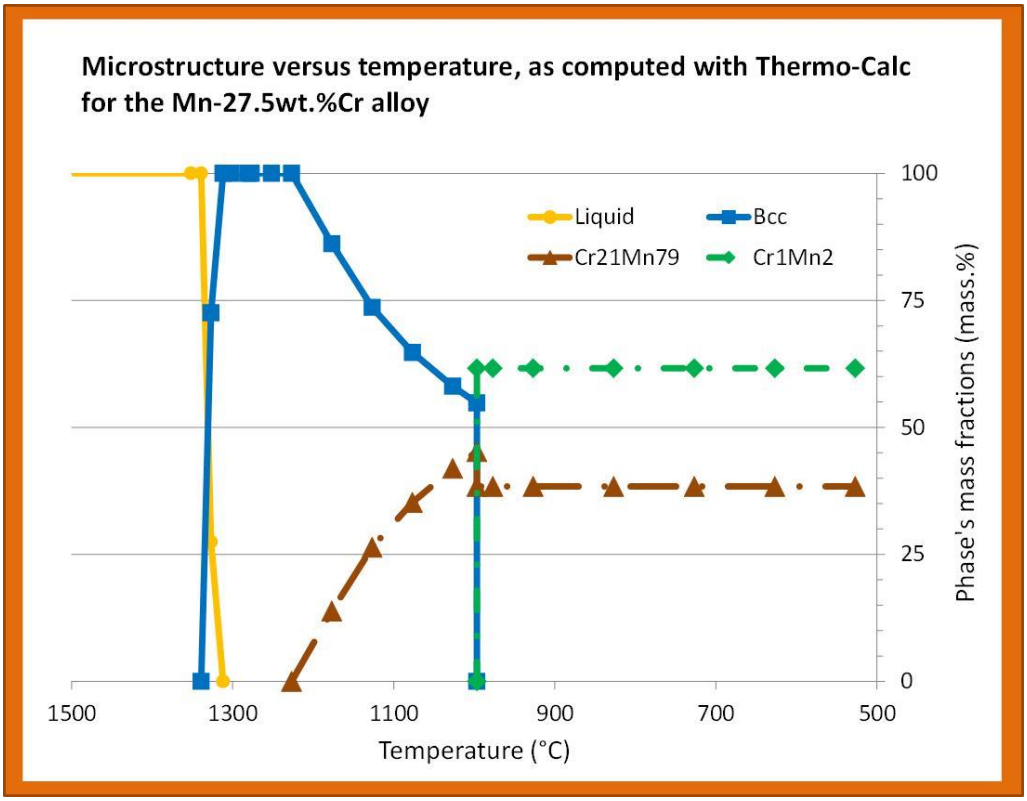

Figure 8. Phase transformations occurring for the MC alloy from 1500°C to 500°C: solidification and solid state cooling (computed by Thermo-Calc N with with KP database)

The calculated evolutions of the chemical compositions of the liquid during solidification and of the BCC Cr–based phase during solidification and during the solid state cooling through the double–phased {Cr_{BCC}, $Mn_{79}Cr_{21}$} domain, are presented in Figure 9 and Figure 10 respectively.

Solidification is obviously accompanied by a positive segregation in manganese and a negative segregation in chromium. At the same time the Cr_{BCC} phase is itself enriched in manganese and impoverished in chromium. During the first part of the solid state cooling the chemical composition of the Cr_{BCC} phase – single phase present – is constant, of course. When the Cr–poor $Mn_{79}Cr_{21}$ intermetallic nucleates and grows at the expense of the Cr_{BCC} phase, the manganese content of the later decreases and its chromium content increases. After the end of the peritectoïd reaction the structure is fixed because of its double–phased constitution of two intermetallic compounds chemically defined, and the compositions of which do not vary, by definition.

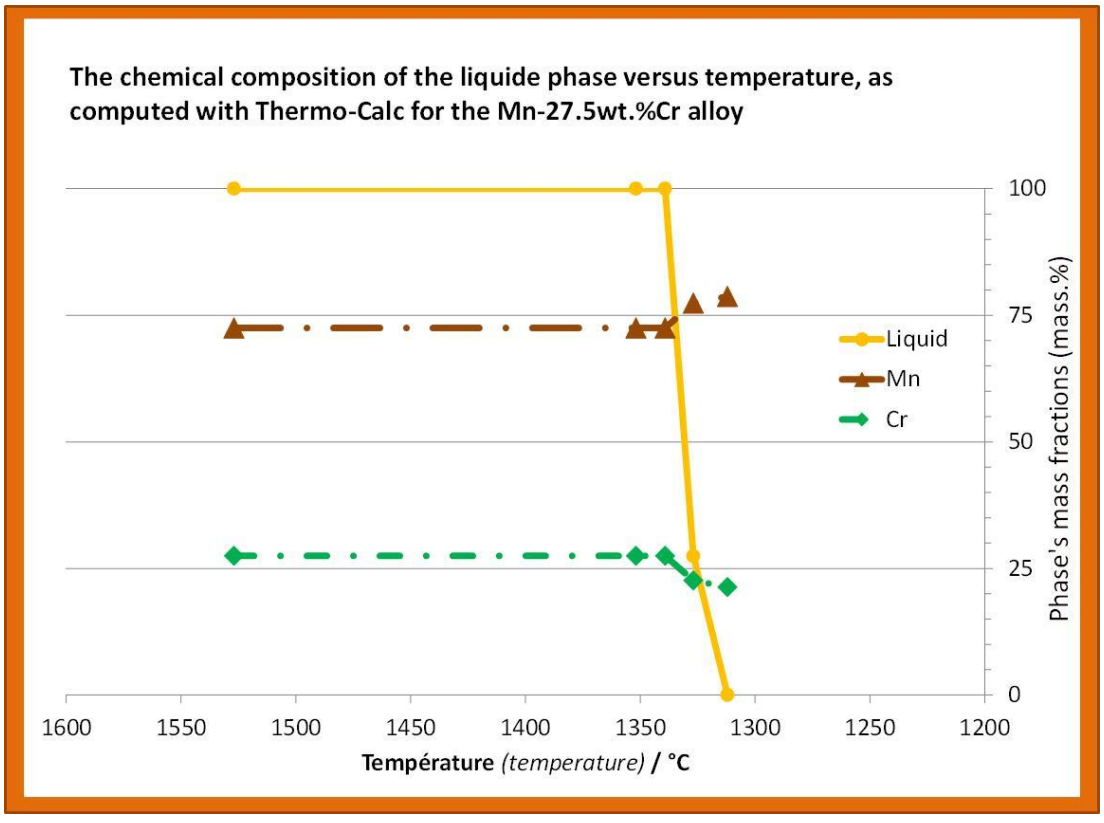

Figure 9. Evolution of the chemical composition of the liquid during the solidification of the MC alloy (computed by Thermo-Calc N with with KP database)

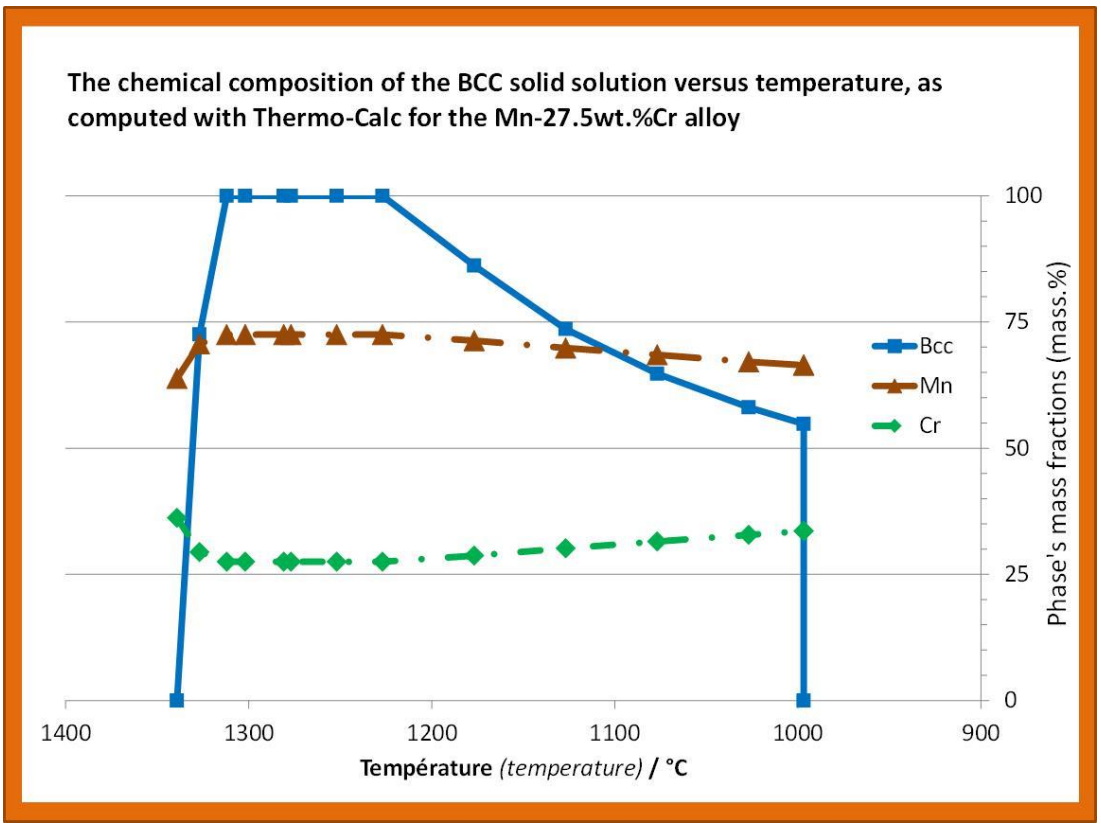

Figure 10. Evolution of the chemical composition of the BCC Cr solid phase, between its appearance at solidification start and its disappearance at the end of the peritectoïd reaction, for the MC alloy (computed by Thermo-Calc N with with KP database)

In the case of the ternary alloys the presence of carbon will influence the solidification, and maybe also the solid state transformations. It was not possible to perform calculations because of the lack of suitable database for system orders higher than 2, but the eutectic–like shaped Cr_7C_3 carbides seen in the as–cast microstructures of some of the present alloys (i.e. with C contents high enough), suggest that a liquid → matrix + Cr_7C_3 may occur at the end of solidification. For the quaternary alloys too poor in tantalum because of a not total dissolution of Ta in the melt before start of cooling, the obtained TaC were not developed enough to allow understanding when they appeared and according to which reaction.

Conclusion

Preceded by initial thermodynamic calculations – necessarily limited because the unavailability of an adequate database – the elaboration of the two series of alloys brought some knowledge about such systems seemingly not explored previously. First the great differences in melting points and in evaporation point between manganese on the one hand, and chromium and tantalum on the other hand, led to elaboration conditions inducing significant evaporation of manganese and to unachieved alloying by tantalum when present. Maybe other elaboration routes, such as powder metallurgy or additive manufacturing, must be preferred to foundry. About the properties of the obtained alloys, some difficulties arose and must be solved before taking benefit of some of the properties of these alloys, their high hardness for example. Indeed hardness typical of water–quenched martensitic steels were obtained without help of many carbides. Certainly, the major problem to solve is the lack of toughness revealed by many micro-cracks discovered after cutting. Future work, in parallel with the characterization of general corrosion and mechanical properties, may consist also in the research of solutions for improving this particular point.

References

[1] F.G. Wilson, B.R. Knott, *Int. J. Powder Metall. Powder Technol.*, 14, 121 (1978).

[2] X.Y. Wang, Y.W. Peng, J.H. Zhang, *Mater. Sci. Eng.*, A, A438-A440, 194 (2006).

[3] T. Hegyes, P. Barkoczy, *Mater. Sci. Forum*, 752, 193 (2013).

[4] K. Stan-Glowinska, *Crystals*, 8, 61/1 (2018).

[5] D. Mukherjee, K. Chidambaram, N. Palaniswamy, M. Valliappan, S.P. Manoharan, K. Balakrishnan, *Bull. Electrochem.*, 6, 499 (1990).

[6] M. Kubota, K. Ono, R.Y. Umetsu, H. Akinaga, A. Sakuma, K. Fukamichi, *Appl. Phys. Lett.*, 90, 091911/1 (2007).

[7] H. Lee, Y.K. Kim, S.C. Yu, *J. Magn. Magn. Mater.*, 254-255, 522 (2003).

[8] Y. Sutou, T. Omori, T. Okamoto, R. Kainuma, K. Ishida, *J. Phys. IV*, 11, 8/185 (2001).

[9] V.G. Gavriljuk, V.V. Bliznuk, B.D. Shanina, S.P. Kolesnik, *Mater. Sci. Eng., A*, A406, 1 (2005).

[10] K. Wakasa, M. Yamaki, *J. Mater. Sci. Lett.*, 10, 925 (1991).

[11] K. Sugawara, S. Ohnuma, T. Masumoto, *Mater. Trans.*, 59, 897 (2018).

[12] T.A. Bhaskaran, R.V. Krishnan, S. Ranganathan, *Bull. Mater. Sci.*, 17, 795 (1994).

[13] A.A. Hamid, P.K. Ghosh, S.C. Jain, S. Ray, *Wear*, 260, 368 (2006).

[14] P. Schafmeister, R. Ergang, *Archiv für das Eisenhüttenweisen*, 12, 507 (1939).
[15] H. Krainer, O. Mirt, *Archiv für das Eisenhüttenweisen*, 15, 467 (1942).
[16] Z. Yang, P. Singh, J.W. Stevenson, G.G. Xia, *J. Electrochem. Soc.*, 153, A1873 (2006).
[17] S. Michon, P. Berthod, L. Aranda, C. Rapin, R. Podor, P. Steinmetz, *Calphad*, 27, 289 (2003).
[18] P. Berthod, L. Aranda, C. Vébert, S. Michon, *Calphad*, 28, 159 (2004).
[19] P. Berthod, Y. Hamini, L. Aranda, L. Héricher, *Calphad*, 31, 351 (2007).
[20] P. Berthod, Y. Hamini, L. Héricher, L. Aranda, *Calphad*, 31, 361 (2007).

HOW TO CITE THIS ARTICLE

Patrice Berthod, Jean-Paul Gomis, Synthia Annick Ozouaki Wora, "**Exploration of the microstructures of two series of chromium–rich Mn–based alloys elaborated by casting**" International Journal of New Chemistry., 2020; 7(4), 318-335. DOI:10.22034/ijnc.2020.669112.1212